New Parameterization of Nonorographic Gravity Wave Scheme for LMDZ6 Mars PCM and Its Impacts on the Upper Atmosphere

Jiandong Liu, Ehouarn Millour, Francois Lott, Antoine Bierjon, Antoine Martinez, Deborah Bardet, Sebastien Lebonnois, Aymeric Spiga, Siteng Fan, **Thomas Pierron , Francois Forget and the LMD Mars PCM Team**, *LMD/IPSL, Sorbonne Université, PSL Research Université, École Normale Supérieure, École Polytechnique,CNRS, Paris, France (jiandong.liu@lmd.ipsl.fr),* ***Gabriella Gilli,*** *Instituto de Astrofisica de Andalucia (IAA), Granada, Spain.*

Overview

To simulate the non-orographic gravity waves' (nonoro-GW) impacts on the Martian upper atmosphere, we have extended the nonoro-GW scheme by Gilli et al. (2020) into the upper atmosphere (i.e. up to the exosphere ~300 km) by revisiting the scheme and adopting a new set of parameters. Secondly, the thermal structure below 100 km simulated by the GCM with the nonoro-GW scheme parametrization is found to be highly consistent with MCS observations. Thirdly, recent improvements in the LMD Mars PCM dust/water cycle model (see Bierjon et al. and Forget et al. talks), coupled to the nonoro-GW scheme, tend to correct some known biases in the modeled thermal tides amplitudes and phases. Additionally, an analysis of the impact of the nonoro-GW parametrization on the thermosphere winds and density (temperature) is described and compared with MAVEN observations.

Introduction

We adapted the non-orographic gravity wave scheme from the LMDZ Earth model, which was first introduced to generate equatorial quasi-biennial oscillation (QBO) (Lott et al., 2012; Lott and Guez, 2013). The core idea of the scheme is first to sample the non-orographic gravity waves (nonoro-GW) spectrum by launching a few monochromatic waves with stochastic selected properties at each model 'physical' time-step. The source of the waves is located just above the top of the convection cells to simulate the nature of real wave packets (Lott et al., 2012). Then, the impact of the waves on the winds is averaged during a day/sol by a 1-order autoregressive (AR-1) algorithm. By this way, these few monochromatic waves can live longer and the wave ensembles can launch at the same location at each time-step.

The scheme has been tested by Gilli et al. (2020) and implemented to the LMDZ5 Mars GCM below 120 km. It has also been transplanted to the LMD Venus and Generic GCMs with different sets of tuned parameters (Gilli et al., 2017 ; Gilli et al., 2020).

In the new scheme, we fixed several bugs and successfully extended the parameterization to Mars upper atmosphere. We came up with a group of newly designed tuning parameters, found after nearly a hundred simulations. We use MRO MCS-derived thermal structure (below 105 km) and several surface rovers pressure/inert gas density observations as constraints to tune the scheme. The impacts of the nonoro-GW on the lower atmospheric thermal structure and on the upper atmosphere are investigated.

Formalism

By using Boussinesq and hydrostatic approximations, the solution of the vertical velocity equation (VVE, See Lott and Guez., 2013) can be expressed by the linear sum of few (8 in the model) monochromatic waves. The waves are designed to have stochastic horizontal wavelengths and phase speeds. They are launched just above the planetary boundary layer (PBL) where the Brunt–Väisälä frequency N^2 changes sign (to positive). The wave packets at the launch altitude have constant Eliassen-Palm (EP)-fluxes and random propagation directions.

The Wentzel-Kramers-Brillouin (WKB) treatment of the VVE is used to pass the vertical wind velocity level by level above the launch altitude. We maintain an overall conserved EP-flux but with minor diffusivity that ensures the waves ultimately dissipate over the last few layers of the model top. Thus, the EP-flux is conveyed from layer z_1 to z_2 as follows:

$$\vec{F}^{z_2} = \frac{\vec{k}\Omega}{|\vec{k}||\Omega|}\Theta[\Omega(z_2)\Omega(z_1)]Min\left\{|\vec{F}^{z_1}|e^{-2\frac{\mu m^3}{\rho\Omega}\delta z}, \rho_r S_c^2 e^{-\frac{z}{H}}\frac{|\Omega|^3 k^{*2}}{2N|\vec{k}|^4}\right\} \quad (1)$$

Where $\vec{F}^z$ is the EP-flux at the altitude z. k is the horizontal wavenumber, where $k_{\min} < k < k_{\max}$. $k^* = 1/\sqrt{\Delta x \Delta y}$, where Δx and Δy are the model horizontal grid dimensions ($\approx 300\ km$).$\Omega = \omega - \vec{k}\vec{u}$ is the intrinsic frequency and $\vec{u}$ the zonal wind.$\omega = \vec{k}c$, c is the wave phase speed. Θ is the Heaviside function where $\Theta = 0$ if $\Omega(z_1)\Omega(z_2) < 0$ to simulate the wave breaking. $\upsilon = \frac{\mu}{\rho}$ is the minor diffusivity applied to the EP-flux amplitude to dissipate the wave at the model top, where μ is the atmospheric viscosity. $m = N\frac{|\vec{k}|}{\Omega}$ is the vertical wavenumber.ρ_r is the atmospheric density at the launch layer. S_c is the saturation number . H is the atmospheric scale height. Once the EP-flux tendency $dF/\rho dz$ is evaluated, we use AR-1 to update the effects on the wind tendency:

$$\left(\frac{\partial \vec{u}}{\partial t}\right)_{GW}^{t+\delta t} = \frac{\delta t}{\Delta t}\frac{1}{M}\sum_{n=1}^{M}\frac{1}{\rho}\frac{dF}{dz} + \frac{\Delta t - \delta t}{\Delta t}\left(\frac{\partial \vec{u}}{\partial t}\right)_{GW}^{t} \quad (2)$$

Where Δt is 24×3600 s (1 sol) and δt is the model physic time-step (=5 min). M=8 is the number of total waves launched at each time step t. Thus, the wind tendency at time $\delta t + t$ (left hand term) is updated by summing current mean tendency (right

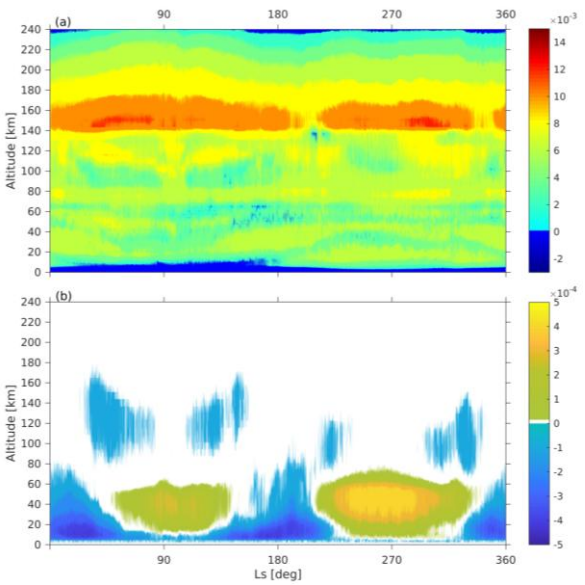

Fig.1 (a) Brunt–Väisälä frequency N^2 and (b) Eliassen-Palm (EP)-fluxes (kg·m^{-1}·s^{-2}) between 30°S and 30°N where the wave packets launched at 5.8 *km* above the surface with EP-flux=5×10^{-4} kg·m^{-1}·s^{-2} and climatology scenario.

hand second term) with the EP-flux tendency that is averaged by both Δt and M (right hand first term).

Parameter Tuning and Comparison with MCS Temperatures

Maximum EP-flux at the launch altitude: As illustrated by equation (1), the scheme launches M (=8) waves just above the PBL (reference layer, *rl*) with EP-flux 0~*EPfm*. As the wave packets pass from one layer to another: (i) the EP-flux dissipates a little bit by a factor of $\frac{\mu}{\rho}$ (left side of the Min {} function of equation (1)). Then, (ii) it compares with the amplitude of a saturated monochromatic wave (SMW), in which the amplitude of the SMW also decreases with altitude by a factor of $e^{-z/H}$. At some altitude, a critical level is reached where the density of the atmosphere is too thin to contain the energy of the waves, therefore, (iii) the intrinsic frequency changes sign and the wave breaks. Around a hundred runs have been made to tune the scheme parameters (Table 1) with respect to MCS temperatures and the model new dust/water cycle. The tunable parameters are as follows:

Table 1. Tunable parameters of the nonoro-GW scheme for LMDZ6 Mars PCM

	EPfm kg·m^{-1}·s^{-2}	S_C	μ m^2 s^{-1}	*kmax* km^{-1}	*kmin* km^{-1}	*Cmax* ms^{-1}	*rl* km
[1]	7×10^{-7}	1.0	10^{-3}	7×10^{-4}	2×10^{-5}	30	8
[3]	5×10^{-4}	1.5	0.07	1×10^{-4}	7×10^{-7}	u_{rl}[2]	6

[1] Gilli et al.(2020); [2]equals to the zonal wind at the reference altitude; [3] LMDZ6

Nonoro-GW launch altitude (*rl*): we have changed the *rl* from 0.4 ($\sigma = P/P_S$) to 0.6 (or from 8 km to 6 km) in the new scheme. The PBL changes very similarly to the critical layer of Brunt–Väisälä frequency N^2. It goes almost down to the ground in the polar region and hits its maximum in the equatorial region with an altitude of 3~10 km (Spiga et al., 2010). The previous *rl*≈8 km causes some cell-like EP-flux structure between the ground and the PBL when we force the downward flux into the surface. Current *rl*≈6 km works well. The AR-1 average is set to 1 sol and the physical time-step has no side effects on the scheme. We are working on changing the *rl* to the exact PBL top and trying to launch the waves excited by other sources such as dust storms and Jet streams. More results will be available in the near future.

Wave phase speed (*Cmin and Cmax*): The *Cmin* is favorable to a small value (~0.1 ms^{-1}). Now the *Cmax* is set as the value of the zonal wind velocity at *rl* , that is, $C_{max} = |u_{rl}|$, make it varying with locations. A constant *Cmax* would overestimate the intrinsic frequency Ω at high latitude while underestimating the value at mid-latitude. As a result, the breaking altitude of the wave packets will be influenced.

Horizontal wavenumber (*kmin and kmax*): The horizontal wavenumber controls the horizontal wavelength by $\lambda_h = 2\pi/k$. As illustrated by Lott et al. (2012), the wavenumber is defined as $k^* < |k| < k_s < N/|u_{rl}|$, where k_s is the horizontal wavenumber of a saturated monochromatic wave. In the previous work made by Gilli et al. (2020), the horizontal wavelength is between10 to 300 km as shown in Table 1. Since we have replaced the k^* in equation (1) with k_{min} to make the amplitude of SMW more sensitive to the parameter tuning process, the previous values induce issues in: (i) the waves in the packets can be launched from a single model grid box (which should not). (ii) the *EPfm* must be a very small value otherwise the waves get saturated extremely fast and break at very lower altitudes, which causes no effect on the model fields.

Saturation and viscosity/dissipation parameters (***S_C and μ***)**:** The amplitude of monochromatic waves (SMW) determines the maximum that the EP-flux can reach. Here we set $S_c = 1.5$ (dimensionless). The viscosity μ or the dissipation μ/ρ is the key factor that can damp the amplitude of the EP-flux at high altitude, which guarantees no more momentum breaks at the model top. We set $\mu = 0.07$ m^{2}s^{-1}for the new scheme.

All our tuning follows the rules below: (i) the tunable parameters should have clear physical definitions and the values should lie within the scope as constrained by the related physical process. (ii) the scheme should not influence the key processes of the model. The surface pressure and the inert gas density should not be changed by the scheme. (iii) the thermal structure/tides of the model with nonoro-

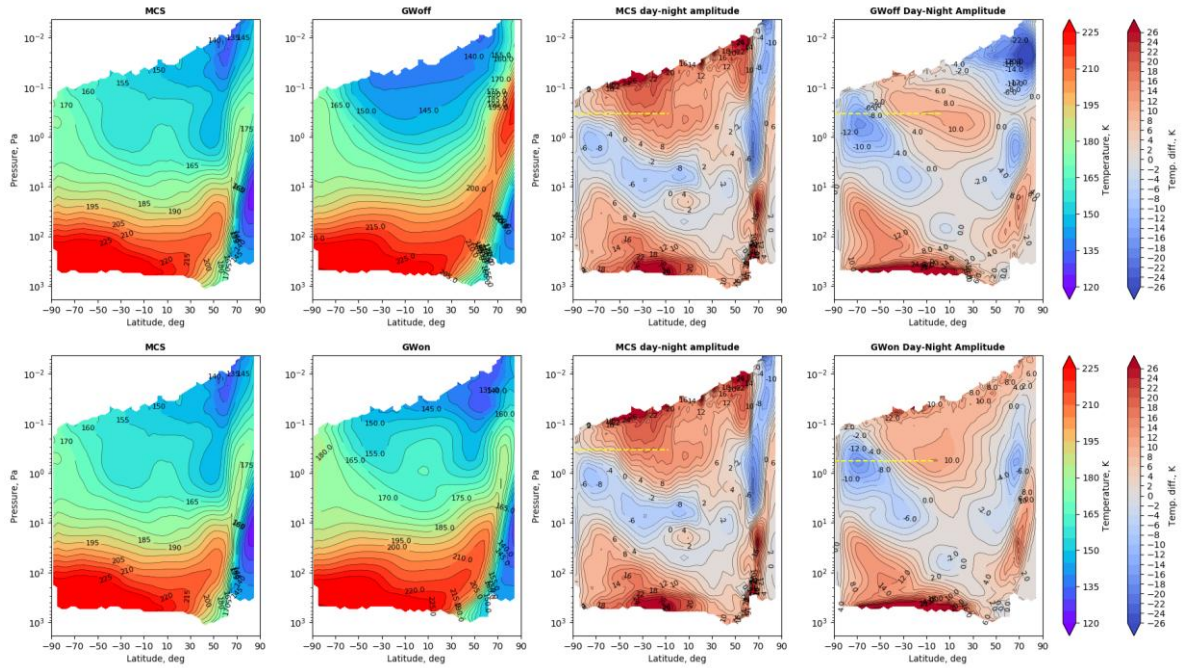

Fig.2 *Upper panels* (*left to right*): MCS observed thermal structure (MY29, Ls 240-270) and the corresponding Mars PCM simulation without nonoro-GW. Thermal tides as seen by MCS and the model results as nonoro-GW turned off. *Lower panels*: same as the upper panels but with nonoro-GW scheme turned on. The model use LMDZ6 new dust/water cycle (see Bierjon et al. *and Forget et al. talks).*

GW turned on should converge to the MCS observations without generating extreme wind shears (>~700 m/s). (iv) the scheme should not be sensitive to the physical time-steps setting.

As illustrated in Fig.2, we use Mars Year 29 (MY29) dust scenario to tune the model. The scheme was first tested in MCD5.3-like dust/water cycle with full model layers including the thermosphere. After a few tens of runs, we found a group of tunable parameters (very close to the one shown in Table 1.) that could make the simulation results comparable with the MCS observation. At the second step, we adopt the parameters to the LMDZ6 Mars PCM that is updated with improved dust-water cycles. Then we tune the scheme based on both the MCD5.3 version parameters and the new dust/water cycle. It is worth to mention that the *Cmax* in the LMDZ6 version is not a tunable parameter anymore as shown in Table 1 compare with MCD5.3 version where we set $C_{max} = 50\ m/s$, which it varies with locations to locations as we take $C_{max} = |u_{rl}|$. The old setting overestimated the phase velocity at latitude higher than 55 degree, thus preventing the model from producing a typical thermal structure in this region.

The nonoro-GW scheme has negligible effects on the model layers that are below altitude of 40 km. The temperature changes due to the nonoro-GWs are less than $|2|$ K below this altitude, which is lower than the model noise (~5 K). The atmosphere in this region is thick enough that the energy released by the breaking waves is absorbed without causing any field disturbances. Indeed, one branching of the wave packets does break at the altitude of 20 km in the equatorial region.

At the same time, the atmospheric fields above 40 km are altered by the gravity waves dramatically. The wave packets launched from the top of the equatorial region breaks at 60-100 km thus generates much more wind fractions than without the waves. This pushes the downward branches of the Hadley cell closer to the poles, in which the polar warming is generated (~25-150 km). Both the zonal and meridional winds are damped by the waves. As a result, it causes 10-20 K temperature variations in the equatorial region and 30-80 K warming (adiabatic heating by the downward branches of the Hadley cell) in the polar region. Besides, some new wind jets with variations ~160 m/s are generated by the waves in latitude between 30°N-70°N, which in turn cool down the air by 30 K.

As we compared the versions 5 and 6 dust/water cycles, we found that the vertical phase of the thermal tides is controlled by the dust cycle. The dust distribution causes temperature increase or decrease in the equatorial region and changes the vertical phase of the tides (2-20 km). Then, the gravity waves cool (where the thermal tides have a positive amplitude) or warm (vice versa) the quadratic structure by order of 10-30 K.

Impacts to the Wind Fields and the Upper Atmosphere

The comparison with MAVEN density is still ongoing. Here we have some primitive investigation of the nonoro-GW in the upper atmosphere. By adding the diffusivity term μ/ρ to the amplitude of

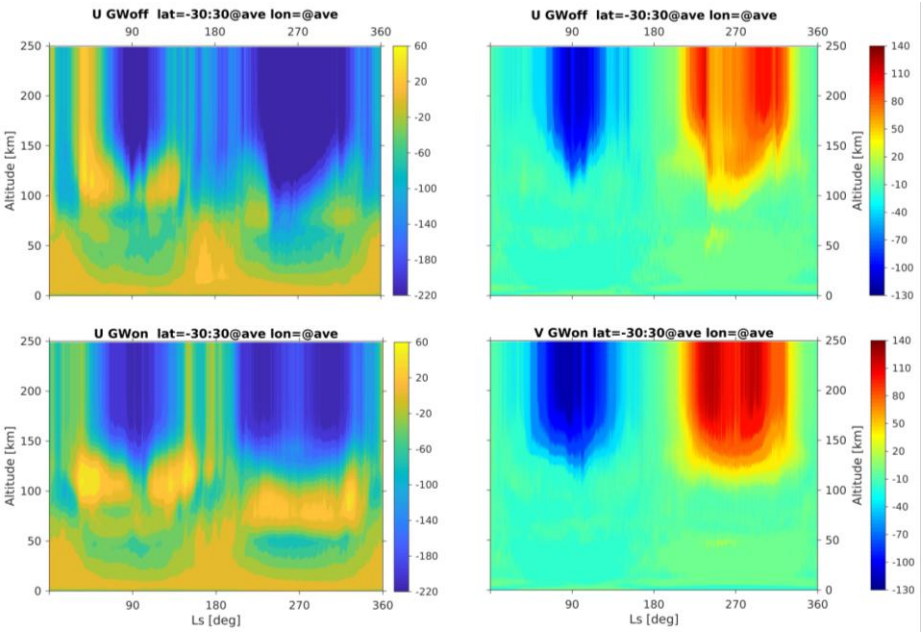

Fig.3 LMDZ6 Mars PCM simulations MY29, Ls 240-270. *Upper*: zonal and meridional winds at equatorial region when nonoro-GW turns off. *Lower*: the same as upper panel but with gravity waves turning on.

the EP-flux, most of the waves break below 140 km (Figure 1.). The wind variations due to the gravity waves can reach 240-360 m/s for zonal direction and 120-180 m/s for meridional direction in the upper atmosphere.

Dramatic temperature changes (~50-80 K) only happen between altitudes of 25-140 km, where the gravity waves-induced wind variations can regulate the circulations, thus generating adiabatic heating. The direct effect of the gravity waves is cooling down the atmosphere by 20 K at altitude 40-140 km.

Above 140 km, the winds vary dramatically and the temperature sees ~20 K changes overall, except for some regions where new wind jets are formed (~>50 K). The density changes are within 30%.

Conclusions

The non-orographic gravity wave scheme of LMDZ6 Mars PCM has been extended to the upper atmosphere. A new group of parameters has been tuned and the simulation results have been compared with the MCS observations. A primitive evaluation of GW on the upper atmosphere is given. The results are as follows:

1) The nonoro-GW effects on the atmosphere below 40 km is minor.
2) Above 40 km, the winds are damped overall and the wind variations due to the waves can reach up to 120-360 m/s while temperature changes vary by 10-80 K.
3) The upper atmospheric wind fields are dramatically influenced. The temperature and density vary ~30 K and ~15%, respectively.

The new scheme has no negative side effects to the surface pressure and the field values match with several rovers' observations. We are investigating to launch the wave packets at the exact PBL altitudes with location variations and waves triggered by other convective sources. The comparison with MAVEN density is ongoing.

Acknowledgements

This work was performed using HPC computing resources from GENCI-CINES (Grant 2021-A0100110391). J.Liu would like to acknowledge the grants support from the China Scholarship Council (CSC).

Reference

G Gilli, F Forget, A Spiga, et al. *JGR: Planets*, 125(3), 2020. doi:10.1029/2018JE005873.

G Gilli, S Lebonnois, F Gonzalez-Galindo, et al. *Icarus*, 281:55–72, 2017. doi: /10.1016/j.icarus.2016.09.016

F Lott, L Guez, and P Maury. *GRL*, 39(6), 2012. doi:10.1029/2012GL051001

F Lott and L Guez, *JGR:Atmosphere*, 118(16):8897–8909, 2013. doi:10.1002/jgrd.50705

Spiga, A., Gonzalez-Galindo, F., Lopez-Valverde, M., and Forget, F. *GRL*, 2012 39, L02201. doi:10.1029/2011GL050343